Physics of Plasmas ARTICLE scitation.org/journal/php

Role of ion thermal velocity in the formation and dynamics of electrostatic solitary waves in plasmas

Cite as: Phys. Plasmas **26**, 042112 (2019); doi: 10.1063/1.5056227
Submitted: 13 September 2018 · Accepted: 20 March 2019 ·
Published Online: 11 April 2019

Amar Kakad,[a] Bharati Kakad,[b] Ajay Lotekar,[c] and G. S. Lakhina[d]

AFFILIATIONS

Indian Institute of Geomagnetism, New Panvel, Navi Mumbai 410218, India

[a]amar@iigs.iigm.res.in
[b]ebharati@iigs.iigm.res.in
[c]ablotekar@gmail.com
[d]gslakhina@gmail.com

ABSTRACT

We perform fluid simulations to examine the effect of ion thermal velocity on the formation and dynamics of solitary waves in an unmagnetized two-component plasma consisting of ions and electrons. Based on the linear and nonlinear fluid theories, some of the previous studies have reported that the plasma with the electron temperature greater than the ion temperature (i.e., $T_e > T_i$) supports ion acoustic solitary waves (IASWs), whereas the plasma with $T_e \ll T_i$ supports electron acoustic waves (EASWs). In this paper, we have considered a wide range of ion temperatures (with fixed electron temperature) to examine the criteria of temperature and thermal velocities in the generation of EASWs and IASWs in plasmas. Our simulation shows that the plasma with $T_i > T_e$ possesses two wave modes depending on the ratio of its thermal velocities. When the ratio of electron to ion thermal velocities $R = V_{the}/V_{thi} > 1$, the system supports the generation of IASWs, whereas for $R < 1$, it supports the generation of EASWs. The analysis of characteristics like the amplitude, width, and phase speed of these solitary waves implies that the EASWs have a negative potential, whereas the IASWs have the positive potential. The transition from IASWs to EASWs occurs when the phase speed of the solitary wave exceeds the limiting value of $\sqrt{3}V_{the}$. This simulation study presents the detailed investigation of the evolution of EASWs and IASWs generated in plasmas having $T_i > T_e$, which will have implications in modeling such waves in space and laboratory plasmas.

I. INTRODUCTION

Fried and Gould[1] obtained the numerical solutions of the linear electrostatic Vlasov dispersion equation in an unmagnetized, homogeneous two-component (electron and ion) plasma and showed the existence of a damped electron acoustic (EA) mode, in addition to the well-known Langmuir and ion acoustic (IA) modes. The EA mode has usually been ignored as it is found to be heavily damped for Maxwellian distributions.[2] Later, it was shown that in the presence of two distinct groups (cold and hot) of electrons and immobile ions, one indeed obtains a weakly damped EA mode, the properties of which significantly differ from those of the Langmuir waves.[3] Based on the theoretical approach, most of the studies related to nonlinear ion- and electron-acoustic waves show that the plasma with the ion temperature much greater than the electron temperature (i.e., $T_i \gg T_e$) supports electron-acoustic solitary waves (EASWs),[4,5] whereas the plasma with ion temperature smaller than the electron temperature supports ion-acoustic solitary waves (IASWs).[6,7] However, the critical temperature ratio of these species required for the existence of the EASWs and IASWs is not known. For multicomponent plasma with one or more ion species which are hotter than some or all of the electron species, the necessary conditions for the generation of large amplitude solitary acoustic modes are discussed by Verheest *et al.*[8] They find that the existence domain of soliton velocities is very narrow and that ions cannot be treated as Boltzmann. Their study indicates that both inertial and thermal effects for the ions need to be kept in such models to study the solitary waves. In our simulation, we have considered both inertial and thermal effects. We find that for the case of hot ion plasma ($T_i > T_e$), depending on the ratio of electron to ion thermal velocity, $R = V_{the}/V_{thi}$, the plasma system supports either IA (when $R > 1$) or EA (when $R < 1$) waves.

The plasma in different regions of the Earth's magnetosphere supports electrons and ions with distinct temperatures. The electrons and ions with $T_i > T_e$ are common in polar cap boundary layer region[9] ring current and the magnetotail region[10,11] of the Earth's

magnetosphere, whereas the Earth's magnetopause and magnetosheath regions support plasma with $T_i < T_e$.[12] Due to these favorable conditions, both EASWs and IASWs are ubiquitously observed in Earth's magnetosphere. These waves have received a great deal of renewed interest as they play an important role in a variety of plasma processes in Earth's magnetosphere, e.g., generation of broadband electrostatic noise,[13,14] particle acceleration processes,[15,16] etc.

In the literature, there are many studies employing multispecies plasma models to examine both IASWs and EASWs. Several researchers have studied the nonlinear IASWs[17–28] and EASWs[11,12,29–38] in multispecies plasmas. But not much attention has been paid to the modelling of the EA waves in two-component (electrons and ions) plasma. There are just a few two-component fluid models with $T_i > T_e$ in the literature which supports electron acoustic waves, e.g., Buti *et al.*[4] and Ghosh *et al.*[5]

Most of the fluid models of the IASWs and EASWs have been studied using the Sagdeev pseudopotential analysis technique, in which the reference frame moves with the solitary wave, for one mode at a time.[36,39] In general, these solitary waves are often referred to as solitons even though the Sagdeev formalism excludes all discussion of their stability and interaction properties. Recently, Kakad *et al.*[6] performed one-dimensional fluid simulations of IASWs and validated this classical theory for the first time for two-component (hot electron and cold ion) plasma. They have shown that the solitary wave solutions obtained from the Sagdeev pseudopotential analysis are stable and in good agreement with the fluid simulations. So far, such fluid simulations are not carried out for EASWs to examine their evolution. The motivation to carry out the present simulation is based on a simple thought. We intend to investigate the generation of solitary wave structures, identify associated wave modes, and examine their evolutionary characteristics in a plasma consisting of ions and electrons obeying $T_i > T_e$. In this paper, we discuss the evolutionary characteristics of the solitary waves formed in the plasma system having different ion thermal velocities. We examined the ion thermal velocity control on the excitation of EASWs to IASWs in plasmas. This paper is structured as follows; the plasma model is briefly discussed in Sec. II. The simulation parameters are discussed in Sec. III. The results obtained from the different simulation runs are elaborated in Sec. IV. The present work is summarized and concluded in Sec. V.

II. PLASMA MODEL

We consider a homogeneous, collisionless, unmagnetized plasma consisting of fluid electrons and fluid ions (H^+). Such a plasma can either support EASWs or IASWs depending on the thermal velocity of the electrons and ions. For the nonlinear waves propagating parallel to the magnetic field along the x-axis, the dynamics of the electrons and ions is governed by the equation of continuity, momentum, and energy for both species and the Poisson equation[6] as follows:

$$\frac{\partial n_j}{\partial t} + \frac{\partial (n_j v_j)}{\partial x} = 0, \tag{1}$$

$$\frac{\partial v_j}{\partial t} + v_j \frac{\partial v_j}{\partial x} + \frac{1}{m_j n_j}\frac{\partial P_j}{\partial x} - \frac{Z_j}{m_j} E = 0, \tag{2}$$

$$\frac{\partial P_j}{\partial t} + v_j \frac{\partial P_j}{\partial x} + \gamma_j P_j \frac{\partial v_j}{\partial x} = 0, \tag{3}$$

$$\epsilon_0 \frac{\partial E}{\partial x} = \sum_j Z_j n_i. \tag{4}$$

The electric field (E) in the equations listed above can be written in terms of an electrostatic potential (ϕ) with the relation $E = -\partial\phi/\partial x$. In the equations listed above, the subscripts $j = e$ and i are used for electrons and ions, respectively. The variables n_j, P_j, and v_j are plasma density, pressure, and velocity of the species j, respectively. Here, m_j and Z_j represent the mass and charge of the species j, respectively. The charge $Z_e = -e$ for electrons and $Z_i = e$ for ions. ϵ_0 is the electric permittivity. For a one-dimensional case, the allowed degree of freedom is 1. Thus, we assume the adiabatic index γ_j as 3 in Eq. (3).

We used the fluid code developed by Kakad *et al.*[6] and solved the unnormalized equations (1)–(4). All physical parameters used in these equations are taken in MKS system. In the simulation code, the spatial derivatives of the quantities in Eqs. (1)–(3) are computed using the finite difference scheme,[6,40] which is accurate up to the fourth order. The Poisson equation is solved using the second-order central finite difference method. We integrate Eqs. (1)–(3) in time by the leap-frog method,[6,40] which is accurate to the second order. The leap-frog method gives rise to a grid separation numerical instability. To eliminate small wavelength modes linked with such numerical instability, we have used a compensated filter.[41] A necessary condition for the convergence of the explicit finite difference method used in our simulation is the Courant condition,[7] $V_{max}\frac{\Delta t}{\Delta x} \leq 1$. Here, Δx and Δt are the space- and time-domain grid size in the simulation and V_{max} is the maximum speed considered in the simulation system. The values of these parameters in the simulations are chosen such that the Courant condition is always fulfilled.

III. SIMULATION PARAMETERS

We perform the fluid simulations in a one-dimensional system with the periodic boundary conditions. For all simulation runs, we assume an artificial electron to ion mass ratio $m_i/m_e = 100$. The flow velocities of the electrons and the ions at $\omega_{pi}t = 0$ are assumed to be zero initially, i.e., $v_{e0}(x) = v_{i0}(x) = 0$. The background electron and ion densities are set in such a way that $n_{e0} = n_{i0} = 1$. Thus, the ion and electron plasma frequencies (ω_{pj}) take values of 0.1 and 1, respectively. We used the localized Gaussian perturbation as an initial density perturbation (IDP) in the equilibrium electron and ion densities given by

$$\delta n = \Delta n \ \exp\left[-\left(\frac{x - x_c}{l_0}\right)^2\right]. \tag{5}$$

In the equation above, Δn and l_0 are the amplitude and width of the superimposed IDP, respectively. Here, $x_c = L_x/2$ is the center of the simulation system. The perturbed densities at the initial time are given by $n_j(x) = n_{j0} + \delta n$. Although the system has quasineutrality (i.e., $n_{e0} = n_{i0}$) at $t = 0$, the gradient in density is not zero, which gets reflected in the thermal pressure of each species. The pressure gradients (i.e., ∇P_j) present in the simulation system act as a free energy source and affect the motion of species through momentum equation (2). Accordingly, different plasma species respond and a finite electric field is generated in the system through charge separation, which grows with time and evolves into solitary waves.

TABLE I. Parameters used in the simulation runs to investigate the effect of ion thermal velocity on the existence domain of EASWs and IASWs. Here, $m_e = 1$ and $m_i = 100$. $L_x = 2 \times 10^5$. We consider $T_e < T_i$ for all the simulation runs.

Run	dx	dt	T_i	V_{thi}	T_e	V_{the}	λ_{di}	Category	Duration for averages
Run-1	1	1×10^{-2}	2	0.1414	1	1	1.41	Category-I	$9000–14\,000\omega_{pe}^{-1}$
Run-2	1	1×10^{-2}	5	0.2236	1	1	2.23	$V_{the}/V_{thi} > 1$	$9000–14\,000\omega_{pe}^{-1}$
Run-3	1	1×10^{-2}	10	0.3162	1	1	3.16		$9000–14\,000\omega_{pe}^{-1}$
Run-4	1	1×10^{-2}	20	0.4472	1	1	4.47		$9000–14\,000\omega_{pe}^{-1}$
Run-5	1	1×10^{-2}	50	0.7071	1	1	7.07		$9000–14\,000\omega_{pe}^{-1}$
Run-6	1	1×10^{-2}	200	1.4142	1	1	14.14	Category-II	$9000–14\,000\omega_{pe}^{-1}$
Run-7	1	1×10^{-2}	400	2.0000	1	1	20.00	$V_{the}/V_{thi} < 1$	$9000–14\,000\omega_{pe}^{-1}$
Run-8	1	1×10^{-2}	500	2.2360	1	1	22.36		$9000–14\,000\omega_{pe}^{-1}$

It may be noted that both electron and ion temperatures play an important role in governing the dynamics of different wave modes formed in two-species plasma systems. For plasmas, where electron temperature is greater than the ion temperature, i.e., $T_e > T_i$, the thermal velocity of electrons is always larger than the ions, i.e., $V_{the} > V_{thi}$, because electrons are less massive as compared to the ions. Such a plasma supports IASWs and Langmuir waves.[6] However, when $T_e < T_i$, we have two possibilities (i) $R = V_{the}/V_{thi} > 1$ and (ii) $R < 1$. So, we performed fluid simulations considering $T_e < T_i$ and varied ion temperature such that we come across both $R > 1$ and $R < 1$ plasma conditions. We fixed $T_e = 1$ for simplicity. As $m_e = 1$, we get electron thermal velocity $V_{the} = 1$. The ion thermal velocity V_{thi} is considered in the range of 2–500, and they are listed in Table I. Out of eight simulation runs, runs 1–5 have $R > 1$ and we consider these runs under category-I. Runs 6–8 have $R < 1$, and we take these simulations runs under category-II. The same IDP is used to perturb the plasma system. For all simulation runs, we took $l_o = 2$ and $\Delta n = 0.03$ (i.e., 3% of ambient plasma density n_0) for IDP, and the system length is taken as $L_x = 2 \times 10^5$. The other parameters used in the simulations are also given in Table I. Here, the physical parameters retrieved from the simulation like density, temperature, thermal velocity, length, and time are expressed in simulation units of $[n_{0e}]$, $[T_e]$, $[V_{the}]$, $[\lambda_{de}]$, and $[\omega_{pe}^{-1}]$, respectively. This is the standard practice used to represent the simulation results.[40,42]

IV. SIMULATION RESULTS

In this section, we discuss one simulation run each from category-I and II. The characteristics of generated solitary wave structures and the mode identification through their dispersion relation are elaborated by analyzing the simulation output. We chose run-2 ($T_i = 5$) from category-I and run-7 ($T_i = 400$) from category-II.

A. Category-I: Evolution of IASWs

In this section, we discuss the evolution of solitary waves generated in the plasma system falling into category-I. The injection of the IDP in the equilibrium electron and ion density generated a very small finite electric field in the system, which evolves into the solitary waves. To get the more insights into the evolution and propagation of these solitary waves, we discuss the spatio-temporal evolutionary characteristics of solitary waves for run 2. It should be noted here that the identification of these generated solitary waves, i.e., whether they are EASWs or IASWs, is verified through their dispersion characteristics in a later part of this section. We identify this mode as IASW. Figure 1 shows the spatial and temporal evolution of the (a) electrostatic potential and (b) electric field for run 2. It should be noted that we use a large system length ($L_x = 2 \times 10^5\ \lambda_{de}$) for the simulation. However, we show only the part of the system length, i.e., from $\pm 5000\lambda_{de}$ in Fig. 1 for the better visualization. Here, $x - x_c = 0$ represents the center of the simulation system. This figure shows that the initial IDP generates a finite potential pulse, which later evolves into two unstable solitary wave pulses and two oscillatory wave packets trapped between them. These unstable pulses become stable at a later time, i.e., their width and amplitude remain nearly constant during their propagation for a sufficiently longer time. The red bands in Fig. 1(a) show electrostatic potential associated with the oppositely propagating solitary wave pulses, whereas the distinct structures around the center of simulation systems are high frequency oscillations that are identified as Langmuir

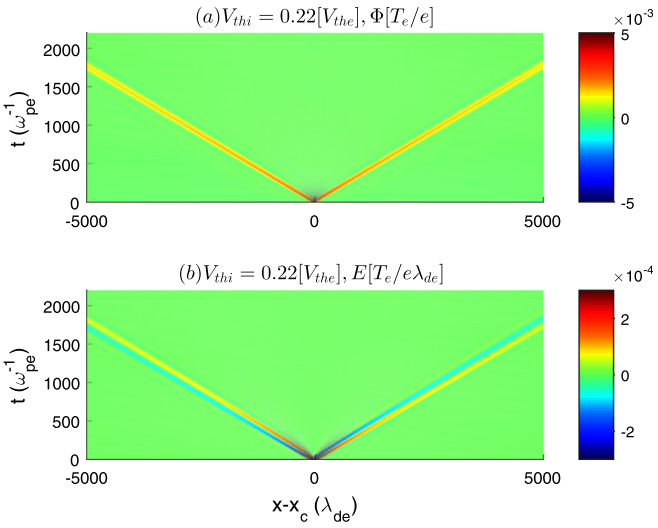

FIG. 1. (a) The spatio-temporal evolution of the electrostatic potential (ϕ) in the system for the simulation run-2 ($V_{thi} = 0.22V_{the}$). In this, the dark red bands correspond to the two oppositely propagating positive amplitude solitary wave pulses, whereas the alternate light blue and yellow circular bands between these pulses are due to the Langmuir oscillations. (b) The spatio-temporal variation of the electric field (E) in the simulation system. The blue and red bands show largely bipolar electric field pulses associated with the solitary waves.

waves. The yellow and blue bands in Fig. 1(b) correspond to the bipolar electric field structures of the oppositely propagating solitary wave pulses. Both solitary pulses are the positive amplitude solitary waves.

To visualize the characteristics of IASWs, we plotted the density and velocity of electrons and ions, and the potential and electric field associated with these IASWs at time $\omega_{pe}t = 5000$ in Fig. 2. Figure 2(a) shows two humps in the electron and ion densities associated with the two IASW pulses that are propagating in the opposite direction away from the center of simulation system. We observed small negative dips in the density at the outer edges of the IASW pulses. In this case, the electron and ion densities are almost identical except a slight difference in their magnitudes around the center of the peaks, where the ion density is slightly greater than the electron density. In panel (b) of Fig. 2, we show the evolution of electron and ion flow velocities at time $\omega_{pe}t = 5000$. We see a dip (i.e., negative v_j) in the electron and ion velocities associated with the IASW pulse propagating along the left direction of the plasma system, whereas the electron and ion velocity pulses associated with the IASW pulse propagating along the right side of the plasma system show a hump (i.e., positive v_j). The dip and hump in velocity are almost identical in shape. However, it is observed that the magnitude of peak ion fluid velocity near the dip and hump is greater than the magnitude of the peak electron fluid velocity. It should be noted that a smaller amplitude velocity fluctuation seen in the electron velocity is associated with the Langmuir oscillations. These fluctuations are seen only in the electron fluid velocity and not in the ion fluid as the Langmuir mode is the high frequency wave mode, which is carried by electrons. The electrostatic potential and the electric field evolved in the system at $\omega_{pe}t = 5000$ are shown in Figs. 2(c) and 2(d), respectively. The positive potential and the largely bipolar characteristics of the electric field associated with the IASWs are evident from this figure. The interesting feature observed here is that the positive potential IASW structures are accompanied by the negative dip at both the edges. Such dips are not associated with the IASWs formed in the plasma with the electron temperature higher than the ion temperature.[6]

Now, we identified the wave modes generated in the simulation. A free energy in the form of IDP at $\omega_{pe}t = 0$ in the system evolves with time, and the energy gets transferred to different wave modes that are excited in the plasma. A standard approach to identify these excited waves in the simulation is to examine their dispersion characteristics by obtaining the ω–k diagram. We obtain the ω–k diagram by taking the Fast Fourier Transformation (FFT) of the electrostatic potential in space and time for run-2. Figure 3 shows the dispersion diagrams of run-2 during (a) $\omega_{pe}t = 0$–200 and (b) $\omega_{pe}t = 500$–700. In this figure, the dashed white lines represent the linear dispersion relation obtained from Eqs. (1)–(4) and the dashed black line shows the electron plasma frequency (ω_{pe}). The slope of these slanted lines is equivalent to the phase velocity of the IASWs estimated from the linear dispersion relation, which is $V_{ph}^{t} = \pm 0.42 V_{the}$. It is seen that the lower dispersion curves extend far below ω_{pe}. This hints that these two dispersion curves are associated with the oppositely propagating IASWs. The upper dispersion curves of the parabolic shape starts at ω_{pe} and extends above ω_{pe}. This is a typical characteristic of the Langmuir waves in unmagnetized plasma.[6] This dispersion analysis indicates that the two solitary wave pulses are IASWs, whereas the dispersive oscillations between these IASW pulses are the Langmuir waves.

We noticed that the characteristic of the Langmuir mode is not the same as the usual Langmuir mode. Linear theory gives the group speed of the Langmuir wave as $V_g = \sqrt{\gamma_e} V_{the}^2 / V_\phi$, where V_ϕ is the

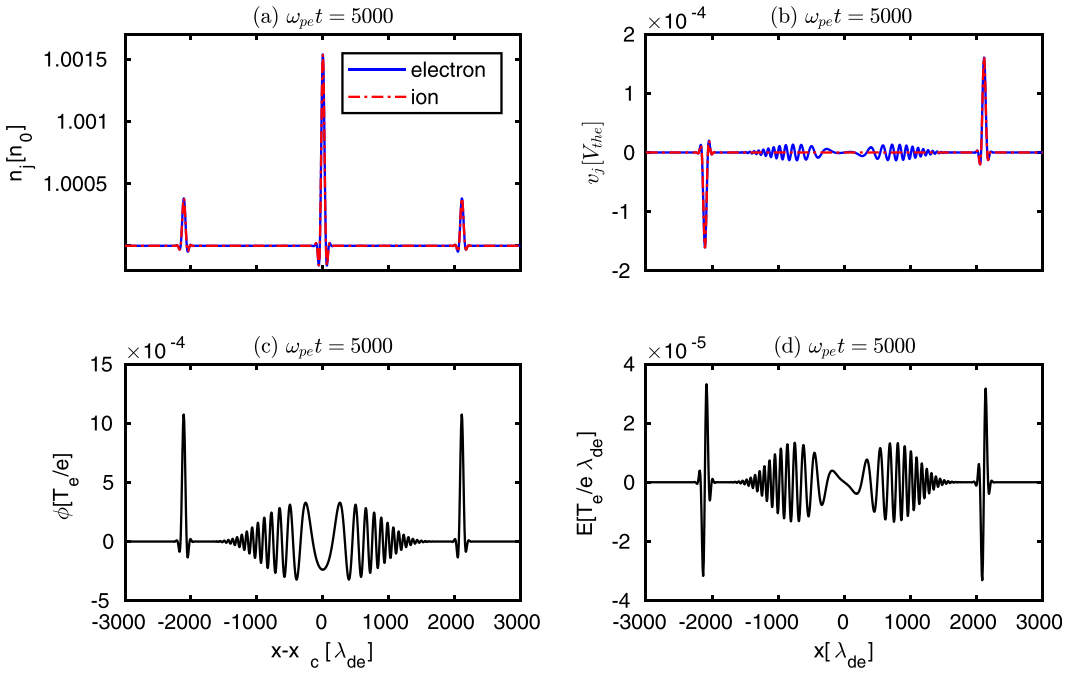

FIG. 2. Evolution of (a) electron and ion density, (b) electron and ion velocity, (c) electrostatic potential, and (d) electric field at $\omega_{pe}t = 5000$ for simulation run-2 (i.e., $T_i = 5$, $T_e = 1$).

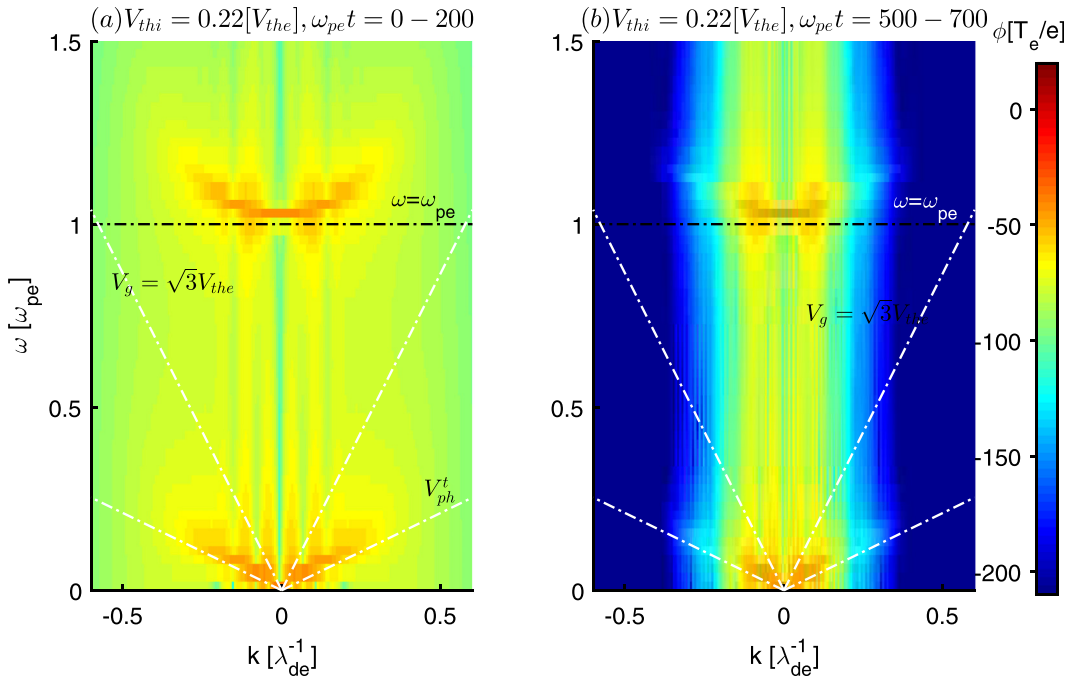

FIG. 3. ω–k dispersion diagrams of electrostatic potential in simulation run-2 during (a) $\omega_{pe}t = 0$–200 and (b) $\omega_{pe}t = 500$–700. It shows two dispersion curves at the bottom, which are due to the IA waves. The upper dispersion curves (above $\omega = \omega_{pe}$) with a parabolic shape are associated with the Langmuir waves. The speed of IASWs estimated from their linear dispersion relation is shown by white dashed-dotted lines in both panels. The electron plasma frequency is shown with the horizontal black dotted line at $\omega = \omega_{pe} = 1$. The power associated with higher wave numbers (k) is reduced significantly during $\omega_{pe}t = 500$–700 in panel (b).

phase speed of the wave. For higher wave numbers, the group speed tends to be $V_g = \sqrt{\gamma_e}V_{the}$ as the phase speed of wave approaches electron thermal velocity. Through computer simulations, it has been demonstrated that in plasmas with $T_e > T_i$, the higher wave number (small spatial scale) oscillations associated with the Langmuir mode indeed propagate with the group speed of $V_g = \sqrt{\gamma_e}V_{the}$, which is much faster than the phase speed of IASWs formed in that plasma system.[6] So, generally, the Langmuir waves are found to be preceded by the IASWs in the spatial domain. However, in the present simulation, it is noted that the smaller amplitude oscillations in the electrostatic potential that are identified as the Langmuir waves are mainly trapped between two oppositely propagating IASWs. In fact, its group speed is much smaller, not exceeding the phase speed of IASWs generated in the system. It implies that the Langmuir wave mode associated with the higher wave numbers is being damped rapidly. Furthermore, it is noted that the small amplitude Langmuir wave oscillations in the electrostatic potential formed in the simulation are associated with the small wave number modes, which are propagating with a group speed much smaller than $\sqrt{\gamma_e}V_{the}$. The ω–k plots shown in Figs. 3(a) and 3(b) indicate that the wave power is limited to smaller wave numbers ($k < 0.2\lambda_{de}^{-1}$) in the later stage of evolution of generated IASWs, i.e., $\omega_{pe}t = 500$–700 as compared to that in the initial stage, i.e., $\omega_{pe}t = 0$–200.

B. Category-II: Evolution of EASWs

The spatio-temporal evolution of electrostatic potential and the electric field for the simulation run-7 is shown in Figs. 4(a) and 4(b),

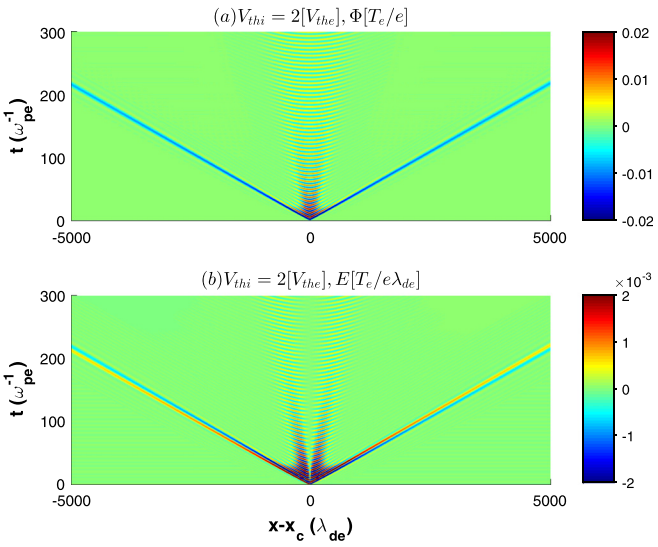

FIG. 4. (a) The spatio-temporal evolution of the electrostatic potential (ϕ) in the system for run-7. In this, the dark blue bands correspond to the two oppositely propagating negative amplitude solitary wave pulses, whereas the circular shaped structures around the center of the system are due to the Langmuir oscillations. (b) The spatio-temporal variation of the electric field (E) in the simulation system. The red and blue bands show largely bipolar electric field pulses associated with the solitary waves.

respectively. The dark blue wide bands in Fig. 4(a) are due to the negative potential associated with the two oppositely propagating solitary wave pulses. Throughout the simulation time, the wide patch around the center of the simulation system shows the propagation of oscillations with distinct wave structures. The spatio-temporal evolution of the electric field in Fig. 4(b) shows the dark blue and red color bands. These bands are due to the bipolar electric field associated with the oppositely propagating solitary wave pulses. In this case, we observe that the oscillations disperse and their amplitude decreases with time, which indicates their dispersive nature. On the other hand, the solitary wave pulses evolve and closely maintain their shape and size in the stability region, i.e., after sufficient time of their generation.

To examine the density and velocity of the electron and ion fluid during the phase when generated EASWs are nearly stable, we plotted their profiles at $\omega_{pe}t = 2000$ in Figs. 5(a) and 5(b), respectively. The electrostatic potential and the electric field during this time are shown in Figs. 5(c) and 5(d), respectively. The electrostatic potential shows two negative amplitude EASW pulses propagating opposite to each other. Small positive potential humps are seen at the left and the right edges of the EASW pulses. Two slowly moving oscillatory Langmuir wave packets in a direction opposite to each other are observed around the center of the system. The electric field associated with these EASW pulses has a largely bipolar form. However, an additional very small amplitude negative (positive) pulse is attached to the left (right) edge of this bipolar electric field pulse. The electron and ion density plot shows two humps propagating opposite to each other. These humps are associated with the EASW pulses generated in the system. The peak electron density is slightly greater than the peak ion density, which maintains the stable bipolar EASW pulses. The electron and ion fluid velocities show the dip associated with the left-side propagating EASW pulse (propagating in the $-x$ direction), whereas the right-side EASW pulse (propagating in the $+x$ direction) shows a hump in the velocity. The peak amplitude of electron velocity is slightly larger than the peak ion velocity. The electron fluid shows smaller amplitude oscillations in their velocity, and they are associated with the Langmuir wave mode.

We obtain the ω–k diagram for run-7 by taking the FFT of the electrostatic potential in space and time. Figures 6(a) and 6(b) show the dispersion diagram of run-7 for $\omega_{pe}t = 0$–200 and $\omega_{pe}t = 500$–700, respectively. In this figure, the dashed black line shows the electron plasma frequency (ω_{pe}). The phase velocity of the EASWs obtained from the linear dispersion relation is $3.46V_{the}$, and it is represented by slanted white dashed lines. In this figure, the upper dispersion curves with a parabolic shape start at ω_{pe} and extend above it. These dispersion curves are similar to the dispersion curve of the Langmuir waves observed in run-2. The lower dispersion curves extend beyond electron plasma frequency (i.e., $\omega > \omega_{pe}$). Such dispersion characteristics are associated with the electron acoustic waves. From Figs. 4 and 6(b), we confirm that the nondispersive solitary pulses are EASWs, whereas the dispersive oscillations between the EASW pulses are Langmuir oscillations propagating slower than the EASWs. Linear theory suggests that the maximum group speed with which the Langmuir wave can propagate is $\sqrt{3}V_{the} = 1.73V_{the}$ and the phase speed of EASW is $V_{ph}^{t} = 3.46V_{the}$. As the Langmuir group velocity is much smaller than

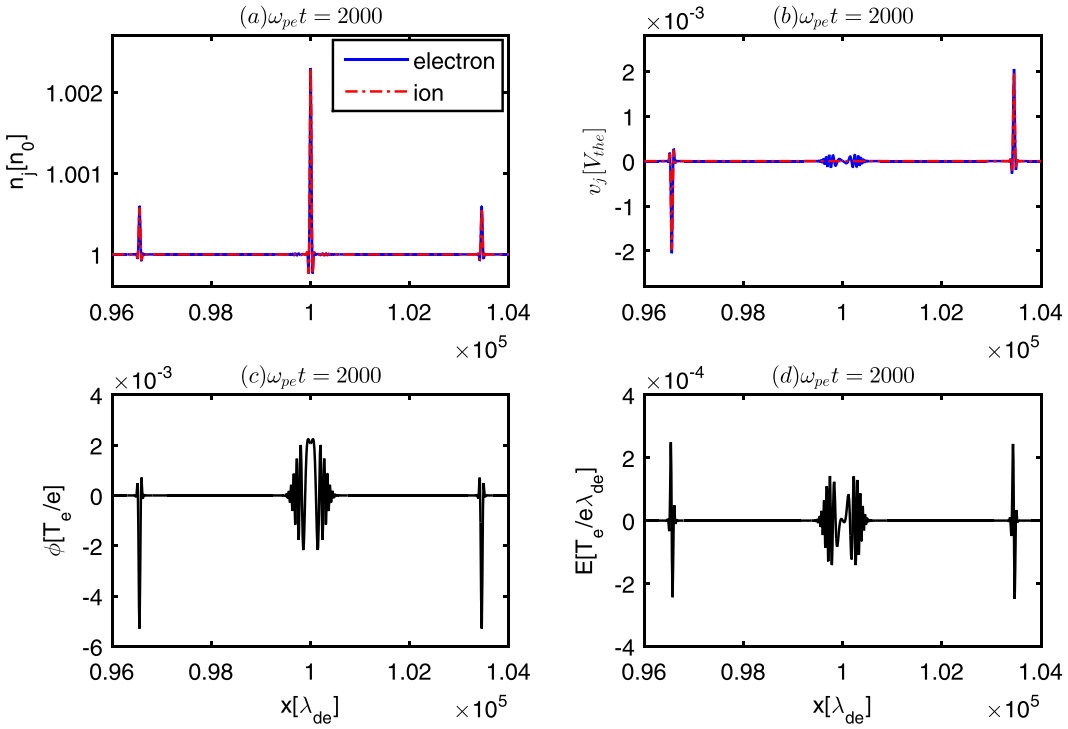

FIG. 5. Evolution of (a) electron and ion density, (b) electron and ion velocity, (c) electrostatic potential, and (d) electric field at $\omega_{pe}t = 2000$ for the simulation run-7 ($T_i = 400$, $T_e = 1$).

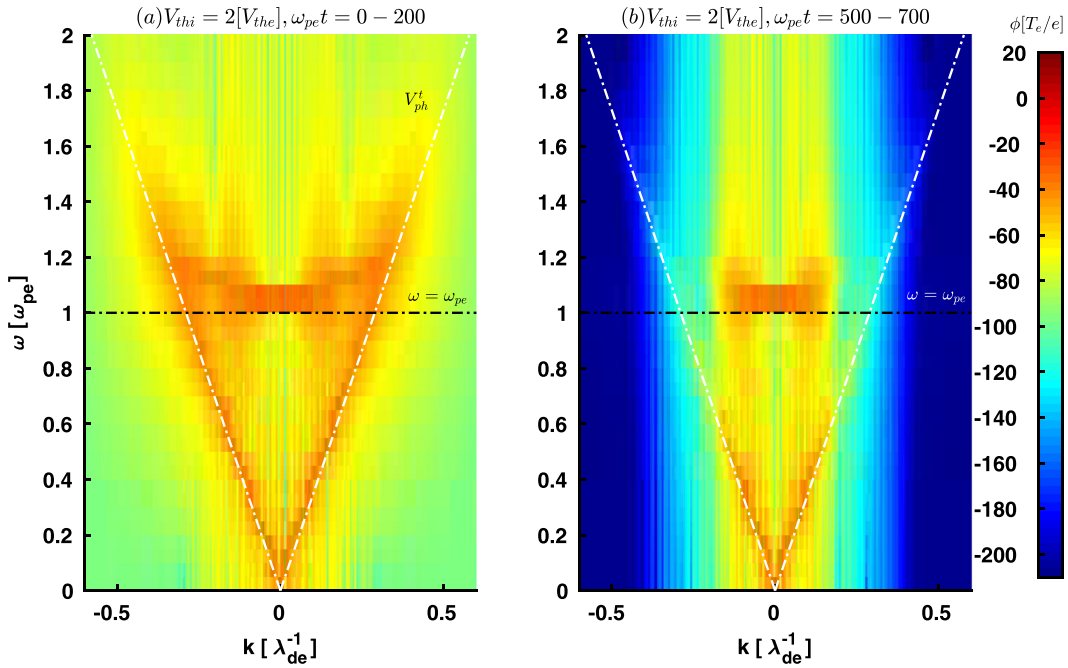

FIG. 6. ω–k dispersion diagrams of electrostatic potential in the simulation run-7 during (a) $\omega_{pe}t = 0$ – 200 and (b) $\omega_{pe}t = 500$–700. It shows two dispersion curves at the bottom, which are due to the EA waves. The upper dispersion curves (above $\omega = \omega_{pe}$) with a parabolic shape are associated with the Langmuir waves. The speed of EASWs estimated from their linear dispersion relation is shown by white dashed-dotted lines in both panels. The electron plasma frequency is shown with the horizontal black dotted line at $\omega = \omega_{pe} = 1$. The power associated with the higher wave numbers (k) is reduced significantly during $\omega_{pe}t = 500$–700 in panel (b).

the phase velocity of the EASWs, the EASWs will be always followed by the Langmuir wave mode in the spatial domain as observed in this plasma simulation. The higher wavenumbers of Langmuir waves are found to undergo nonlinear damping for this simulation run-7 like for simulation run-2.

C. Characteristics of solitary waves in categories-I and II

In this section, we examine the characteristics of the solitary waves such as their phase speed, amplitude, and width in both categories-I and II. For the simulation runs 1–8, we have estimated the average amplitude, phase speed, and width of IASWs and EASWs during the time period, where these solitary waves are nearly stable. The time periods over which these averages are computed are given in Table I. The standard deviation in the average estimates of amplitude, phase speed, and width of solitary waves is in the range of 3%–4%, 0.1%–0.8%, and 2%–3%, respectively, over a time span of $5000\omega_{pe}$. As the standard variation in these parameters is small, we can consider these solitary pulses to be nearly stable. First, we plotted the average phase velocity of the solitary wave pulses and their associated maximum electrostatic potential in Fig. 7. It is seen that the phase velocity of the IASWs decreases with the increase in peak electrostatic potential, and the phase velocity of the EASWs increases with the increase in peak electrostatic potential. The transition from EASWs to IASWs imposes the limit of $\sqrt{3}V_{the}$ on the phase speed of these solitary waves. It means that the EASWs (IASWs) travel with phase speed greater (smaller) than $\sqrt{3}V_{the}$. Here, a factor of $\sqrt{3}$ appears because the adiabatic index for electrons is $\gamma_e = 3$. The EASWs evolved in the simulations have negative potential, whereas the IASWs have positive potential. We examine the width-amplitude dependence for both categories, i.e., for IASWs and EASWs. Figure 8 depicts the average width and average maximum amplitude of the IASWs (black circles) and EASWs (red filled dots) for different simulation runs given in Table I. It is seen from this figure that the width of the IASWs has tendency to increase with the increase in potential, whereas for EASWs, it shows a slight decrease with the increase in the amplitude. However, the overall effect of ion temperature on the width is not significant.

To summarize the effects of ion thermal velocity on the existence and characteristics of EASWs and IASWs, we plotted the phase velocity (V_s) and the maximum amplitude (ϕ_m) of these waves as a function of ion thermal velocity in Fig. 9. The red dashed vertical line depicted at $V_{thi}/V_{the} = 1$ in both panels divides categories-I and II. We can say that (i) $V_{thi} < V_{the}$ even when $T_i > T_e$ supports the IASWs, whereas (iii) $V_{thi} > V_{the}$ supports the EASWs. It may be noted that $T_i < T_e$ always supports the IASWs and such plasma systems are studied earlier through fluid simulations.[6] When $T_e > T_i$, the V_{thi}/V_{the} is always less than $\sqrt{m_e/m_i}$. In the present study, we have considered the artificial mass ratio while performing simulations and the limiting value of $\sqrt{m_e/m_i}$ comes out to be 0.1. It is seen from Fig. 9(a) that the phase speed of both IASWs and EASWs is directly proportional to the ion thermal velocity. We observe that the simulation runs under category-I support positive amplitude IASWs, whereas runs from category-II support negative amplitude EASWs. The maximum amplitude (ϕ_m)

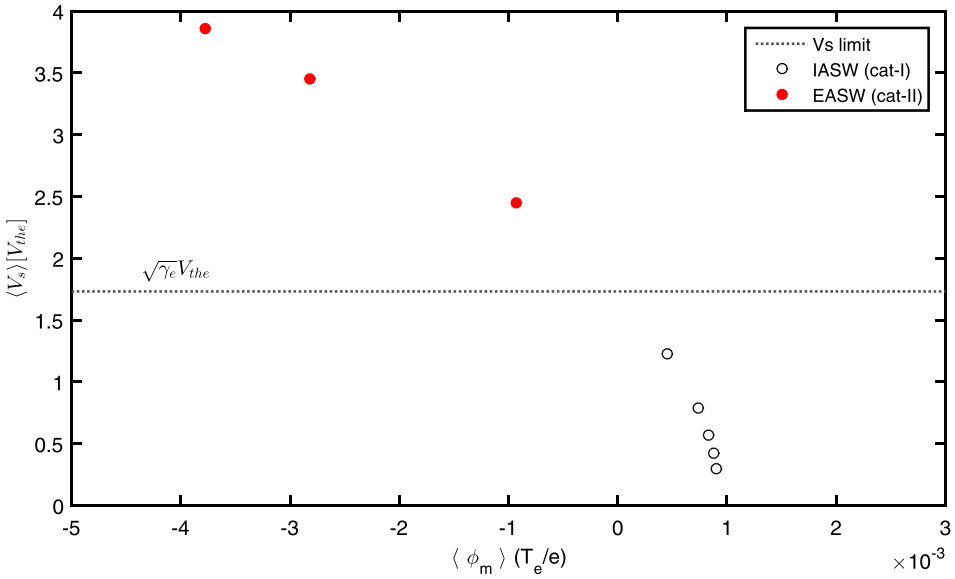

FIG. 7. The phase speeds of IASWs and EASWs as a function of its peak amplitude for simulation runs 1–8. The transition from EASWs to IASWs takes place at $V_s = \sqrt{3}V_{the}$. It suggests that the EASWs (IASWs) travel with a phase speed higher (lower) than $\sqrt{3}V_{the}$.

of the IASWs decreases with the increase in ion thermal velocity, whereas the maximum amplitude ($|\phi_m|$) of the EASW increases with the increase in the ion thermal velocity.

Next, we have carefully examined the spatial variation of the potential and electric field associated with solitary structures that are in the nearly stable stage. For each simulation run, we chose the solitary wave propagating in the $+x$ direction during its stability, and the corresponding spatial variation of the electrostatic potential and electric field is plotted in Fig. 10. In this figure, panels (a) and (b) show the electrostatic potential of the IASWs and EASWs, respectively. The electric fields associated with the IASWs and EASWs are shown in panels (c) and (d), respectively. To compare their variations, each solitary pulse is plotted in such a way that its maximum potential is placed at $x = 0$. An interesting feature can be seen in this figure. The electrostatic potential associated with both IASWs and EASWs generated in plasma with

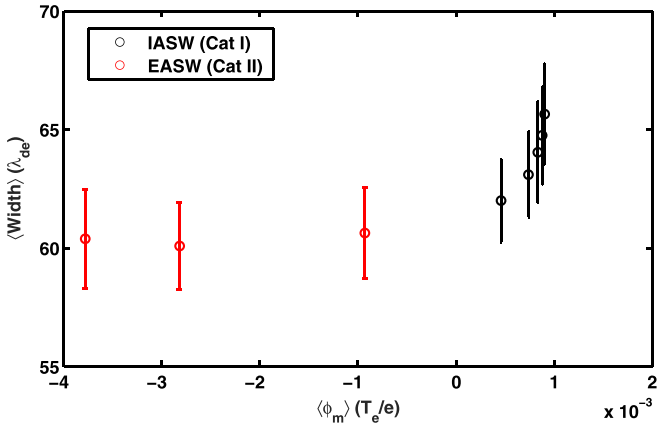

FIG. 8. The width of IASWs and EASWs as a function of their peak amplitude for the simulation runs 1–8. The width of the EASWs decreases with the increase in its amplitude, whereas the width of the IASWs increases with the increase in its amplitude.

$T_i > T_e$ possesses additional smaller amplitude dips and humps, respectively, at the edges of these solitary structures. Such humps or dips are generally not seen in the stable solitary structures commonly termed as solitons. Also, the profiles obtained from the Sagdeev pseudopotential theory for such a plasma system do not support the presence of such humps or dips near the edges of solitary wave structures. The presence of these smaller amplitude humps or dips at the edges of EASWs or IASWs does not affect the stability of these solitary structures.

V. CONCLUSIONS

We have performed the one-dimensional fluid simulations of the solitary waves propagating parallel to the magnetic field in an electron-ion plasma by considering a sufficiently large system length. We considered a plasma system having $T_i > T_e$. We find that in such a plasma system the IDP supports the generation of either IASWs or EASWs depending on the ratio, R, of electron to ion thermal velocities. The characteristics like the amplitude, width, and phase speed of solitary waves are also controlled by the parameter R. Some of the earlier studies have proposed that the plasma with $T_i > T_e$ supports the EA wave mode.[1,4,5] We find that the condition $T_i > T_e$ is not the sufficient condition for the existence of the EASWs in plasma. Due to the different masses of the electron and ion, $T_i > T_e$ does not always mean that $V_{thi} > V_{the}$ (i.e., $R < 1$); it can also give $V_{thi} < V_{the}$ (i.e., $R > 1$). Our simulation shows that the necessary condition for the existence is governed by their thermal velocities and it supports the generation of EASWs only if $V_{thi} > V_{the}$. In such a system, the ions with higher thermal velocity provide restoring force, while electrons with lower thermal velocity provide inertia to support the electron acoustic waves. In the plasma systems having $V_{thi} < V_{the}$, the electrons provide restoring force due to their higher thermal velocity, whereas the ions provide inertia to support IASWs in plasma. The transition from EASWs to IASWs imposes the limit of $\sqrt{\gamma_e}V_{the}$ on the phase speed of these solitary waves. This means that the EASWs (IASWs) travel with phase speed greater (smaller) than $\sqrt{\gamma_e}V_{the}$. The EASWs evolved in the two species plasma have a negative potential, whereas the IASWs have a positive potential.

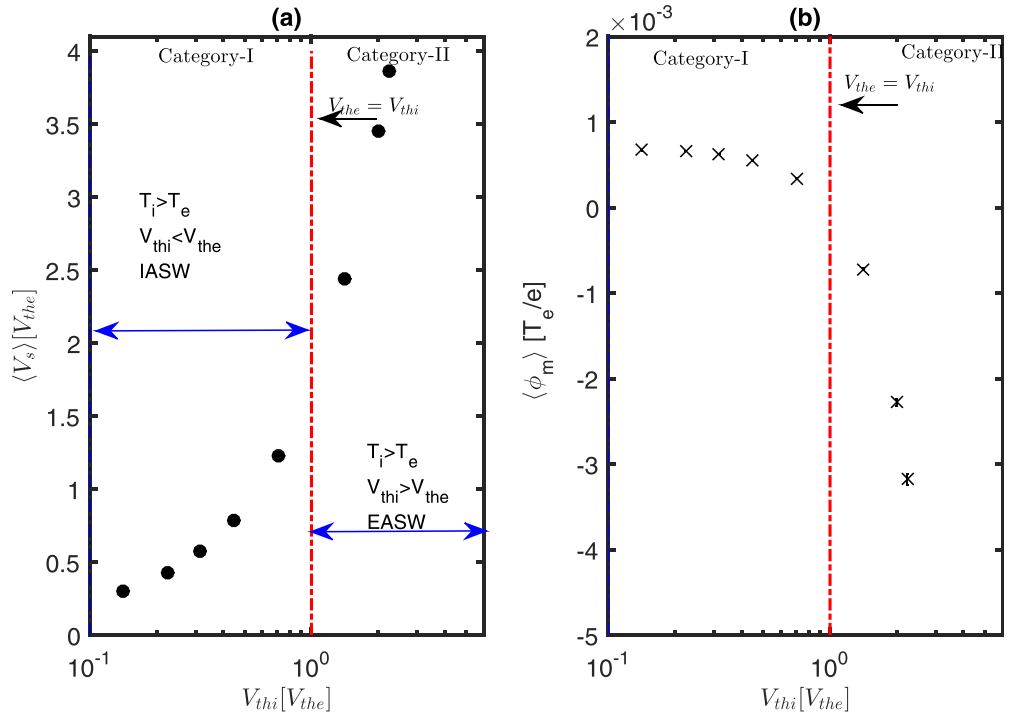

FIG. 9. (a) The phase speed and (b) peak amplitude of IASWs and EASWs as a function of ion thermal velocity for simulation runs 1–8. The vertical dotted line represents the limit where the ion thermal velocity equals the electron thermal velocity, i.e., $V_{thi} = V_{the}$. When $V_{thi} < V_{the}$, we observe IASWs, whereas $V_{thi} > V_{the}$ supports EASWs.

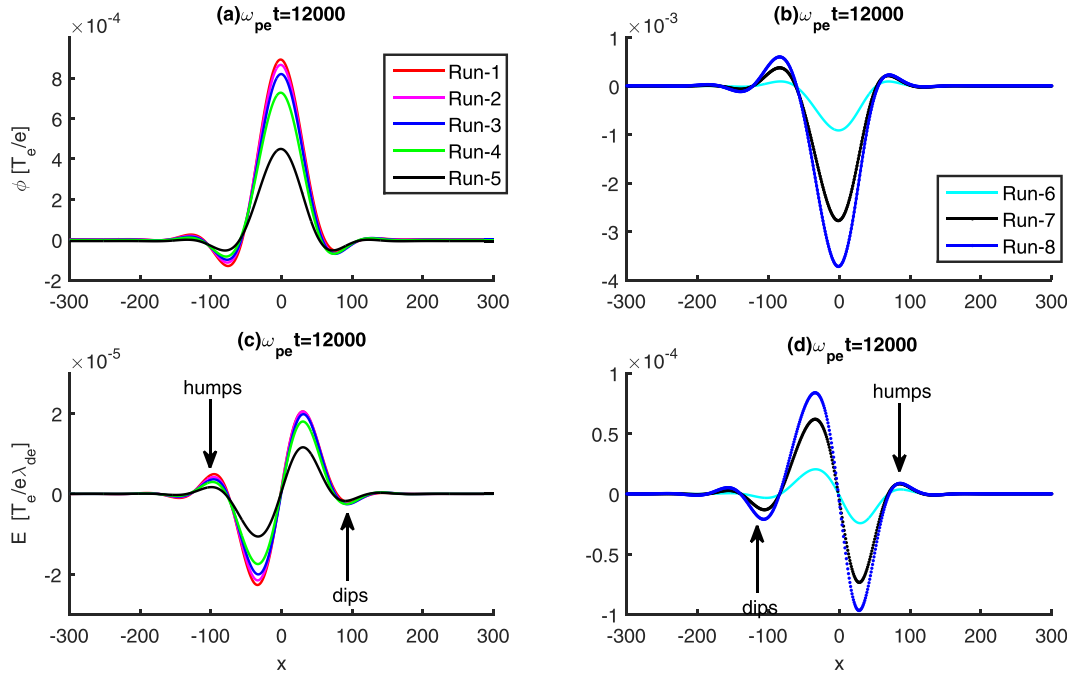

FIG. 10. (a) and (b) Electrostatic potential and (c) and (d) corresponding electric field profiles associated with IASWs (runs 1–5) and EASWs (runs 6–8) during their stability are shown. Here, $x = 0$ represents the position of peak in potential structures for each profile associated with the IASWs and EASWs.

For both EASWs and IASWs, the phase speed of these solitary waves is found to be proportional to the ratio of ion thermal velocity to electron thermal velocity, i.e., $V_s \propto V_{thi}/V_{the}$. It is seen that the peak amplitude of potential associated with the EASWs (IASWs) increases (decreases) with an increase in the ion thermal velocity. When $V_{thi}/V_{the} < 1$, IASWs are formed in the plasma, and as this ratio starts approaching values closer to one, the IA mode amplitude decreases drastically. When the ratio V_{thi}/V_{the} exceeds one, there is a transition from IASWs to EASWs. For the case of $T_i < T_e$, the condition $V_{thi}/V_{the} < 1$ is automatically satisfied. Such plasma systems are well examined through fluid simulations,[6] and they always support the generation of IASWs in addition to Langmuir waves. Thus, to summarize, we can say that the condition (i) $V_{thi} < V_{the}$ supports the IASWs, and (ii) $V_{thi} > V_{the}$ supports the EASWs.

The fluid simulations presented in this paper give the details of evolution of IASWs and EASWs generated in plasma having $T_i > T_e$. It is noted that most of the early studies of modeling EASWs are based on the Sagdeev pseudopotential method that predicts only the stationary EA solitary wave solutions, where the soliton conditions are accomplished. It does not provide information about the transition process through which the stable EA solitons are generated in the electron-ion plasma. The present simulation uses the standard initial perturbation in equilibrium electron and ion densities, which evolves into either EASWs or IASWs in the plasma. The Langmuir wave mode is also generated in the system; however, the higher wave number Langmuir wave modes are found to be heavily damped. One additional feature revealed by this simulation study is that the electrostatic potential associated with the IASWs (EASWs) generated in such plasma is associated with an additional smaller amplitude dips (humps) at the edges of these solitary structures. Such humps or dips are not seen in the stable solitary structures commonly termed as solitons. The presence of such humps or dips is not present in the solitary wave profiles obtained from the Sagdeev pseudopotential theory for such plasma systems. We find that the presence of these smaller amplitude humps or dips at the edges of EASWs or IASWs does not affect the stability of these solitary structures. We speculate from the density profiles of the solitary waves that the humps and dips around the outer edges of their potential pulse are developed due to the accumulation of the electron and ion fluid in those regions. Such humps and dips are also seen in the solitary waves captured by a spacecraft in the Earth's magnetosphere.[12,43]

Generally, the localized perturbations in plasma are produced in a laboratory by very high laser powers and are known to be responsible for the generation of solitary waves in plasmas. In space, the density perturbations can originate in the Earth's magnetospheric regions, such as bow shock, magnetopause, and magnetosheath driven by solar wind variations. These regions of the magnetosphere support electrons and ions with $R < 1$ and $R > 1$, which is favourable for the generation of both EASWs and IASWs. In this context, the present simulations will be helpful to model spacecraft observations of EASWs and IASWs in the Earth's magnetosphere.

ACKNOWLEDGMENTS

The model computations were performed on the High Performance Computing System at the Indian Institute of Geomagnetism. G.S.L. thanks the Indian National Science Academy, New Delhi, for the support under the INSA-Honorary Scientist Scheme.

REFERENCES

[1]B. D. Fried and R. W. Gould, Phys. Fluids **4**, 139 (1961).
[2]S. P. Gary and R. L. Tokar, Phys. Fluids **28**, 2439 (1985).
[3]K. Watanabe and T. Taniuti, J. Phys. Soc. Jpn. **43**, 1819 (1977).
[4]B. Buti, M. Mohan, and P. Shukla, J. Plasma Phys. **23**, 341 (1980).
[5]S. Ghosh, A. Sen, and G. Lakhina, Nonlinear Processes Geophys. **9**, 463 (2002).
[6]A. Kakad, Y. Omura, and B. Kakad, Phys. Plasmas **20**, 062103 (2013).
[7]A. Kakad and B. Kakad, Phys. Plasmas **23**, 122101 (2016).
[8]F. Verheest, M. Hellberg, and G. Lakhina, Astrophys. Space Sci. Trans. **3**, 15 (2007).
[9]B. Tsurutani, J. Arballo, G. Lakhina, C. Ho, B. Buti, J. Pickett, and D. Gurnett, Geophys. Res. Lett. **25**, 4117, https://doi.org/10.1029/1998GL900114 (1998).
[10]C.-P. Wang, M. Gkioulidou, L. R. Lyons, and V. Angelopoulos, J. Geophys. Res.: Space Phys. **117**, A08215 (2012).
[11]A. Kakad, S. Singh, R. Reddy, G. Lakhina, and S. Tagare, Adv. Space Res. **43**, 1945 (2009).
[12]G. Lakhina, S. Singh, A. Kakad, M. Goldstein, A. Vinas, and J. Pickett, J. Geophys. Res.: Space Phys. **114**, A09212 (2009).
[13]H. Matsumoto, H. Kojima, T. Miyatake, Y. Omura, M. Okada, I. Nagano, and M. Tsutsui, Geophys. Res. Lett. **21**, 2915, https://doi.org/10.1029/94GL01284 (1994).
[14]Y. Omura, H. Kojima, and H. Matsumoto, Geophys. Res. Lett. **21**, 2923, https://doi.org/10.1029/94GL01605 (1994).
[15]F. Mozer, S. Bale, J. Bonnell, C. Chaston, I. Roth, and J. Wygant, Phys. Rev. Lett. **111**, 235002 (2013).
[16]I. Vasko, O. Agapitov, F. Mozer, J. Bonnell, A. Artemyev, V. Krasnoselskikh, G. Reeves, and G. Hospodarsky, Geophys. Res. Lett. **44**, 4575, https://doi.org/10.1002/2017GL074026 (2017).
[17]H. Washimi and T. Taniuti, Phys. Rev. Lett. **17**, 996 (1966).
[18]B. Buti, J. Plasma Phys. **24**, 169 (1980).
[19]M. Hudson, W. Lotko, I. Roth, and E. Witt, J. Geophys. Res.: Space Phys. **88**, 916, https://doi.org/10.1029/JA088iA02p00916 (1983).
[20]R. Bharuthram and P. Shukla, Phys. Fluids **29**, 3214 (1986).
[21]M. Berthomier, R. Pottelette, and M. Malingre, J. Geophys. Res.: Space Phys. **103**, 4261, https://doi.org/10.1029/97JA00338 (1998).
[22]R. Reddy and G. Lakhina, Planet. Space Sci. **39**, 1343 (1991).
[23]G. Lakhina, S. Singh, and A. Kakad, Phys. Plasmas **21**, 062311 (2014).
[24]C. Olivier, S. Maharaj, and R. Bharuthram, Phys. Plasmas **22**, 082312 (2015).
[25]A. Kakad, B. Kakad, C. Anekallu, G. Lakhina, Y. Omura, and A. Fazakerley, J. Geophys. Res.: Space Phys. **121**, 4452, https://doi.org/10.1002/2016JA022365 (2016).
[26]A. Kakad, A. Lotekar, and B. Kakad, Phys. Plasmas **23**, 110702 (2016).
[27]A. Lotekar, A. Kakad, and B. Kakad, Phys. Plasmas **23**, 102108 (2016).
[28]A. Lotekar, A. Kakad, and B. Kakad, Phys. Plasmas **24**, 102127 (2017).
[29]R. Mace and M. Hellberg, Phys. Plasmas **8**, 2649 (2001).
[30]N. Dubouloz, R. Treumann, R. Pottelette, and M. Malingre, J. Geophys. Res.: Space Phys. **98**, 17415, https://doi.org/10.1029/93JA01611 (1993).
[31]M. Berthomier, R. Pottelette, M. Malingre, and Y. Khotyaintsev, Phys. Plasmas **7**, 2987 (2000).
[32]S. Singh and G. Lakhina, Planet. Space Sci. **49**, 107 (2001).
[33]A. Kakad, S. Singh, R. Reddy, G. Lakhina, S. Tagare, and F. Verheest, Phys. Plasmas **14**, 052305 (2007).
[34]G. Lakhina, A. Kakad, S. Singh, and F. Verheest, Phys. Plasmas **15**, 062903 (2008).
[35]G. S. Lakhina, S. Singh, and A. Kakad, Adv. Space Res. **47**, 1558 (2011).
[36]F. Verheest and M. A. Hellberg, Phys. Plasmas **22**, 072303 (2015).
[37]S. Chowdhury, S. Biswas, N. Chakrabarti, and R. Pal, Phys. Plasmas **24**, 062111 (2017).
[38]L. Mbuli, R. Bharuthram, and S. Maharaj, Phys. Plasmas **25**, 012318 (2018).
[39]R. Z. Sagdeev, "Cooperative phenomena and shock waves in collisionless plasmas," in *Reviews of Plasma Physics*, edited by M. Leontovich (Consultants Bureau, New York (1966), Vol. 4, pp. 23–91.
[40]B. Kakad, A. Kakad, and Y. Omura, J. Geophys. Res.: Space Phys. **119**, 5589, https://doi.org/10.1002/2014JA019798 (2014).
[41]Y. Omura and J. L. Green, J. Geophys. Res.: Space Phys. **98**, 9189, https://doi.org/10.1029/92JA02901 (1993).
[42]H. Matsumoto and Y. Omura, *Computer Space Plasma Physics: Simulation Techniques and Software* (Scientific Publishing Company, Tokyo, Japan, 1993).
[43]J. Pickett, L.-J. Chen, S. Kahler, O. Santolik, M. Goldstein, B. Lavraud, P. Décréau, R. Kessel, E. Lucek, G. Lakhina, *et al.*, Nonlinear Processes Geophys. **12**, 181 (2005).